

# Generation of PTEN-knockout (-/-) murine prostate cancer cells using the CRISPR/Cas9 system and comprehensive gene expression profiling

AKIKO TAKAO<sup>1</sup>, KAZUHIRO YOSHIKAWA<sup>2</sup>, SIVASUNDARAM KARNAN<sup>1</sup>, AKINOBU OTA<sup>1</sup>, HIROTSUGU UEMURA<sup>3</sup>, MARCO A. DE VELASCO<sup>4</sup>, YURIE KURA<sup>3</sup>, SUSUMU SUZUKI<sup>5</sup>, RYUZO UEDA<sup>6</sup>, TOKIKO NISHINO<sup>2</sup> and YOSHITAKA HOSOKAWA<sup>1</sup>

<sup>1</sup>Department of Biochemistry, Aichi Medical University School of Medicine;

<sup>2</sup>Division of Research Creation and of Biobank, Research Creation Support Center, Aichi Medical University, Nagakute, Aichi 480-1195; Departments of <sup>3</sup>Urology, and <sup>4</sup>Genome Biology, Kindai University Faculty of Medicine, Osaka-Sayama, Osaka 589-8511;

<sup>5</sup>Division of Research Support, Research Creation Support Center, <sup>6</sup>Department of Tumor Immunology, Aichi Medical University School of Medicine, Nagakute, Aichi 480-1195, Japan

Received December 15, 2017; Accepted July 30, 2018

DOI: 10.3892/or.2018.6683

**Abstract.** Phosphatase and tensin homolog (PTEN) deficiency is associated with development, progression, and metastasis of various cancers. However, changes in gene expression associated with PTEN deficiency have not been fully characterized. To explore genes with altered expression in *PTEN*-deficient cells, the present study generated a PTEN-knockout cell line ( $\Delta$ PTEN) from a mouse prostate cancer-derived cell line using the clustered regularly interspaced short palindromic repeats (CRISPR)/CRISPR-associated protein 9 (CRISPR/Cas9) gene editing system. Following transfection of the CRISPR/Cas9 construct, DNA sequencing was performed to identify deletion of the *Pten* locus and PTEN inactivation was verified by western blotting. The  $\Delta$ PTEN cell line exhibited enhanced RAC-alpha serine/threonine-protein kinase phosphorylation and cyclin D1 expression. In addition, an increase in cell proliferation and colony formation was observed in the  $\Delta$ PTEN cell line. Gene expression profiling experiments were analyzed with microarray and microRNA (miRNA) arrays. In the microarray analysis, 111 genes exhibited  $\geq 10$ -fold increased expression compared with the parent strain and mock cell line and 23 genes were downregulated. The only

miRNA with increased expression of 10-fold or more was mmu-miR-210-3p. Genes with enhanced expression included genes involved in the development, progression, and metastasis of cancer such as Tet methylcytosine dioxygenase 1, twist family BHLH transcription factor 2, C-fos-induced growth factor and Wingless-Type MMTV Integration Site Family, Member 3, and genes involved in immunosuppression such as Arginase 1. The results of the present study suggest that PTEN deficiency mobilizes a variety of genes critical for cancer cell survival and host immune evasion.

## Introduction

Phosphatase and tensin homolog (PTEN) is a tumor suppressor and a lipid phosphatase that catalyzes dephosphorylation of phosphatidylinositol 3,4,5-trisphosphate. PTEN has a high frequency of mutations in various cancers including prostate cancer and glioblastoma. PTEN alterations are observed in approximately half of all malignant tumors and correlate with increased RAC-alpha serine/threonine-protein (AKT) phosphorylation and initiation of downstream targets that modulate a wide range of cellular processes associated with the progression of tumor growth and survival (1-8).

To investigate the function of PTEN, various knockout mice have been prepared and the effect of PTEN deficiency examined (9). The authors also established a conditional PTEN-deficient mouse model of prostate cancer driven by the *PSA-Cre* promoter and demonstrated its utility in various experimental settings (10-13). To develop better treatment strategies requires a deeper understanding the cellular and molecular mechanisms of PTEN deficiency. However, autochthonous tumors are highly heterogeneous and are composed of a complex tumor microenvironment that consists of various cell types including epithelial cancer cells, stromal fibroblasts, immune endothelial and blood cells, in addition to other

---

*Correspondence to:* Dr Kazuhiro Yoshikawa, Division of Research Creation and of Biobank, Research Creation Support Center, Aichi Medical University, 1-1 Yazakokarimata, Nagakute, Aichi 480-1195, Japan

E-mail: yoshikaw@aichi-med-u.ac.jp

**Key words:** phosphatase and tensin homolog, clustered regularly interspaced short palindromic repeats/CRISPR-associated protein 9, gene editing, microarray, microRNA arrays

contaminants, all of which contribute to the molecular characterization of PTEN deficiency. Although small interfering RNA methodology enables us to induce PTEN-deficiency at the protein level (14), researchers often take into consideration the fact that gene expression still remains at a certain level even under conditions of gene knockdown.

Next-generation genome editing strategies have been developed and are currently considered some of the best technological tools to most efficiently characterize gene function (15). The present study generated an isogenic PTEN-deficient cell clone from a parental mouse prostate cancer cell line using the clustered regularly interspaced short palindromic repeats (CRISPR)/CRISPR-associated protein 9 (CRISPR/Cas9) system and performed comprehensive gene expression profiling analyses to identify its impact on unique genes associated with crucial roles in cellular processes, including cancer development and immunity.

## Materials and methods

**Cell lines.** The mouse prostate cancer cell line, 2924V, which expresses wild-type PTEN was used in the present study. This cell line was established from a prostate tumor originating from a 57 week-old *PSA<sup>Cre</sup>;Pten<sup>loxP/loxP</sup>* conditional knockout mouse (10). Cells were cultured at 37°C and 5% CO<sub>2</sub> in RPMI-1640 medium (Sigma-Aldrich; Merck KGaA, Darmstadt, Germany) supplemented with 10% inactivated fetal bovine serum (HyClone; GE Healthcare Life Sciences, Logan, UT, USA), 100 IU/ml penicillin, and 100 µg/ml streptomycin.

**PTEN-knockout using the CRISPR/Cas9 system.** The CRISPR/Cas9 system was used to disrupt the expression of the PTEN gene as described previously (16). pSpCas9(BB)-2A-Puro (PX459) was a gift from Feng Zhang (Broad Institute of MIT, Harvard, MA, USA; Addgene plasmid #48139; 15). Briefly, a single guide RNA (sgRNA) sequence was selected using Optimized CRISPR Design (<http://crispr.mit.edu/>). The sgRNA sequence targeting PTEN was 5'-GCTAACGATCTCTTTGATGA-3'. The plasmid expressing human Cas9 and the PTEN sgRNA was prepared by ligating oligonucleotides into the *BbsI* site of PX459 (Pten/PX459). To establish a PTEN knockout clone with a one-nucleotide deletion, 2924V cells (1x10<sup>6</sup> cells/dish) were seeded in a 10-cm dish. Cells were then transfected with 10 µg of PTEN/PX459 using Lipofectamine<sup>®</sup> 3000 (Thermo Fisher Scientific, Inc., Waltham, MA, USA). Antibiotic selection (puromycin; 2 µg/ml) was begun 72 h after transfection and continued for at least 3 days. A single clone was selected, expanded, and then used for biological assays. For sequence analysis of the PTEN gene, the following primer set was used: 5'-CGCTAATCCAGTGTACAGTA-3' and 5'-CTGCGAGGATTATCCGTCTT-3'.

**Morphology.** The cells were plated in a 12-well plate. After 24 h, the cell morphology was digitally photographed at x100 magnification using an inverted microscope system (IX73; Olympus Corporation, Tokyo, Japan).

**MTT assay.** Briefly, parent cells, mock cells, and ΔPTEN were seeded (5x10<sup>3</sup> cells/well) into a 96-well plate. Subsequently, 10-µl MTT solution (5 µg/ml; Sigma-Aldrich; Merck KGaA,

Darmstadt, Germany) was added to each well and cells were incubated at 37°C in 5% CO<sub>2</sub> for 4 h. Next, cell lysis buffer [10% sodium dodecyl sulfate (SDS) in 0.01 M HCL] was added to the wells to dissolve the formazan crystals produced by MTT. The optical density (550 nm) at each time point (day 0, 1, 3, 5, and 7) is presented as the mean ± standard error of the mean (n=6).

**Colony formation assay.** Colony formation assays were performed by seeding 500 cells of each line in 12-well plates. After 14 days, cells were fixed/stained with 3.7% formaldehyde (Wako Pure Chemical Industries, Ltd., Osaka, Japan) containing 0.2 % (wt/vol) crystal violet (Sigma-Aldrich; Merck KGaA) at room temperature and number of colonies were imaged and counted manually. Bar graphs represent the number of stained colonies. Data are presented as the mean ± standard error of the mean (n=3).

**Western blotting.** Cells were lysed in radioimmunoprecipitation assay buffer (Wako Pure Chemical Industries, Ltd.) supplemented with a protease inhibitor cocktail (Roche Applied Science, Mannheim, Germany) for 30 min at 4°C. Insoluble material was removed by centrifugation at 15,400 x g for 10 min at 4°C. Protein content was determined using a DC protein assay kit (5000112JA; Bio-Rad Laboratories, Inc., Hercules, CA, USA) according to the manufacturer's protocol. Protein lysates were mixed with loading buffer and boiled for 5 min. A total of 10 µg protein was separated by electrophoresis on 10% PAGE gels (TEFCO, Tokyo, Japan). Proteins were then transferred to Immobilon-P membranes (EMD Millipore, Billerica, MA, USA) and blocked in 5% skim milk in Tris-buffered saline with 0.01% Tween-20 (TBS-T) for 1 h at room temperature. All antibodies were purchased from Cell Signaling Technology, Inc. (Danvers, MA, USA). Membranes were incubated with primary antibodies [PTEN, 1:3,000, #9559; AKT1, 1:1,000, #9272; phosphorylated (p)-AKT, 1:1,000, #9271; phosphorylated (p)-Rb, 1:3,000, #9307; cyclin D1, 1:3,000, #2922; CDC2, 1:3,000, #9112; CDK2, 1:3,000, #2546; CDK4, 1:3,000, #2906; CDK6, 1:1,000, #3136; CDK7, 1:1,000, #2916 and GAPDH 1:5,000, #5174] overnight at 4°C. After three washes with TBS-T, membranes were incubated with anti-mouse, #7076/rabbit, #7074, horseradish peroxidase (HRP)-conjugated secondary antibody (1:5,000) for 1 h at room temperature followed by a final wash. Proteins were detected by applying ImmunoStar LD (Wako Pure Chemical Industries, Ltd.) to the membrane and signals were quantified using ImageQuant LAS-4000 (GE Healthcare Life Sciences, Little Chalfont, UK) according to the manufacturer's protocol.

**RNA extraction.** For microarray analysis, reverse transcription (RT)-polymerase chain reaction (PCR) and quantitative (q) PCR, total RNA was extracted from cell lines with the NucleoSpin RNA kit (Macherey-Nagel, Düren, Germany) according to the manufacturer's protocol. RNA extraction for miRNA analysis was performed with the miRNeasy Mini Kit (Qiagen GmbH, Hilden, Germany) according to the manufacturer's protocol.

**Microarray analysis.** Expression profiling analysis of mRNA was performed using the Agilent Oligo Microarray Kit (8x60 K;

Table I. Primers used for polymerase chain reaction.

Gene name	Accession	Relative intensity of KO/mock	Forward primer	Reverse primer
<i>Tet1</i>	NM_001253857	32	ACACAGTGGTGCTAATGCAG	AGCATGAACGGGAGAATCGG
<i>Twist2</i>	NM_007855	13	TACAGCAAGAAATCGAGCGAAG	GCTGAGCTTGTTCAGAGGGG
<i>Arg1</i>	NM_007482	12	CTCCAAGCCAAAGTCCTTAGAG	GGAGCTGTCATTAGGGACATCA
<i>Figf</i>	NM_010216	10	AACAGATCCGAGCAGCTTCTA	TTTTGAGCTTCAACCGGCATC
<i>Wnt3</i>	NM_009521	10	AGCGTAGCAGAAGGTGTGAAG	CCAGGTGGCCCCCTTATGATG
<i>Galnt14</i>	NM_027864	-19	CTCATCAAACCTGCTCCCACA	GCTCTGGATCACCGTACTGC
<i>Ptgr1</i>	NM_025968	-30	CAATCGTTCCTTTTGGGAAG	CATGAGAGTTGCAGCCAAAA

Tet1, Tet methylcytosine dioxygenase 1; Twist2, twist family BHLH transcription factor 2; Arg1, Arginase 1; Figf, c-fos induced growth factor; Wnt3, Wnt family member 3; Ptgr1, prostaglandin reductase 1; Galnt14, polypeptide N-acetylgalactosaminyltransferase 14.

G4852B; Agilent Technologies, Inc., Santa Clara, CA, USA). Nucleic acid labeling and hybridization were performed with the One-Color Microarray-Based Gene Expression Analysis kit (Agilent Technologies, Inc.) according to the manufacturer's protocol. Briefly, 100 ng of total RNA was amplified and labeled using the Low Input Quick Amp Labeling Kit. After labeling, RNA was purified with RNeasy Mini Kit (Qiagen GmbH). The RNA fragmentation reaction was performed at 60°C for 30 min, after which the samples were collected on ice for 1 min, and 2X Hi-RPM Hybridization Buffer was added to stop the reaction. Samples were further mixed, centrifuged at 13,000 x g for 1 min at room temperature, placed on ice, and then loaded onto the array. The arrays were hybridized at 65°C for 17 h. The microarray slides were then washed with Gene Expression Wash Buffers I and II and scanned with the Agilent Microarray Scanner-G2505C (Agilent Technologies, Inc.). Feature Extraction Software Version 11.0.1.1 (Agilent Technologies, Inc.) was used to extract and analyze the signals and signal intensities were normalized as previously described (17).

The background signals were normalized and microarray expression data were rank-ordered according to the expression levels of the  $\Delta$ P TEN/mock cells. Differentially expressed genes between  $\Delta$ P TEN and mock cells were considered relevant if there was  $\geq 10$ -fold change.

Functional enrichment analyses of differentially expressed genes were carried out using the Panther web-based tool (18).

To confirm gene expression, RT-qPCR was performed using the ABI 7900 HT Fast Real-Time PCR System (Applied Biosystems; Thermo Fisher Scientific, Inc.) and calculated using the  $2^{-\Delta\Delta C_t}$  method (19). Total RNA from the three cell lines were converted to cDNA with the High Capacity cDNA Reverse Transcription Kit (Applied Biosystems; Thermo Fisher Scientific, Inc.) according to the manufacturer's protocol. The Tet methylcytosine dioxygenase 1 (*Tet1*), twist family BHLH transcription factor 2 (*Twist2*), arginase 1 (*Arg1*), C-fos induced growth factor (*Figf*), Wingless-Type MMTV Integration Site Family, Member 3 (*Wnt3*), prostaglandin reductase 1 (*Ptgr1*), polypeptide N-acetylgalactosaminyltransferase 14 (*Galnt14*), and GAPDH (reference) genes were amplified and detected using SYBR-Green (Applied Biosystems; Thermo Fisher Scientific, Inc.). PCR reactions were prepared in a final volume of 20  $\mu$ l, with 17.6  $\mu$ l of SYBR-Green PCR

Master Mix (Applied Biosystems; Thermo Fisher Scientific, Inc.), 2.0  $\mu$ l of DNA, and 0.2  $\mu$ l each of the 10 pmol/ $\mu$ l forward and reverse primers. Thermal cycler settings included DNA polymerase activation at 95°C for 2 min followed by 55 cycles of denaturation at 95°C for 15 sec, annealing at 60°C for 15 sec, and extension at 70°C for 20 sec. Each measurement was performed in triplicate. The quality of the PCR products was monitored by using the post-PCR melt-curve analysis.

In order to visualize PCR Products, PCR was carried out changing the number of cycles to 30 cycles. The PCR products were electrophoresed in 1.5% agarose gel, and stained with GelRed Nucleic Acid Stain (41003-T; Biotium, Inc., Fremont, CA, USA) and photographed. Primer sequences are listed in Table I.

*miRNA array analysis.* miRNA profiling analysis was performed using the Agilent Mouse miRNA kit (8x60 K; G4872A-070155). miRNA labeling, hybridization, and washing were carried out according to the manufacturer's protocol (Agilent Technologies, Inc.). Hybridized microarrays were scanned with a DNA microarray scanner (Agilent Microarray Scanner; G2505C) and features were extracted using the Agilent Feature Extraction image analysis tool (version 11.0.1.1). Briefly, average values of the spots of each miRNA were background-subtracted and subjected to further analysis. miRNA array expression data were rank-ordered according to the expression levels of the  $\Delta$ P TEN/mock cells. To confirm miRNA expression level, RT-qPCR was performed. Total RNA from the three cell lines were converted to cDNA with the Taqman MicroRNA Reverse Transcription Kit (Applied Biosystems) according to the manufacturer's protocol. Realtime PCR was performed using Taqman MicroRNA Assays (has-miR-210, RT:000512 and snoRNA234; RT:001234 as control; Applied Biosystems) according to the manufacturer's protocol.

*Statistical analysis.* At least three replications per experiment and three independent experiments were performed. The results are expressed as the mean  $\pm$  standard error of the mean. Independent-samples Student's t-test and one-way analysis of variance, followed by the least significant difference post-hoc test were performed to analyze data using JMP Ver.13.2.1

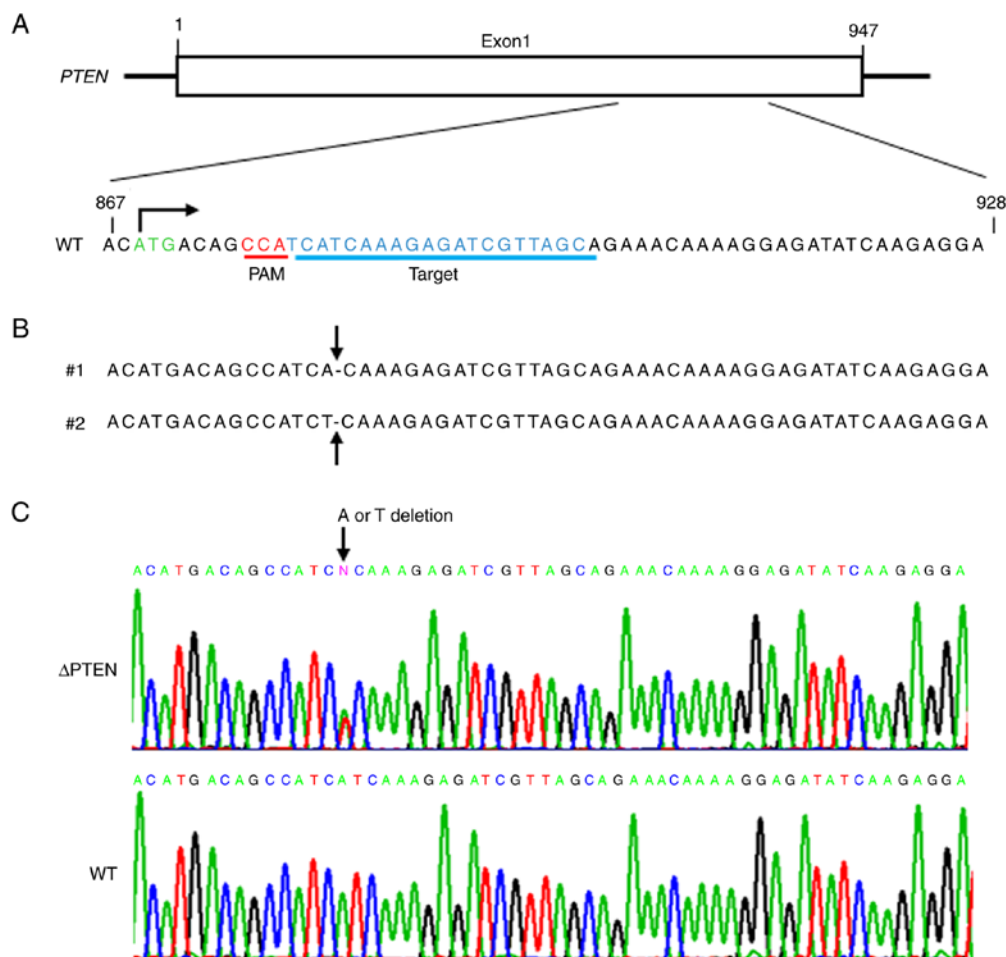


Figure 1. Generation of a *PTEN*-knockout cell line using the CRISPR/Cas9 gene editing system. (A) An sgRNA sequence was designed against the mouse *PTEN* gene to delete a nucleotide in the target sequence indicated by the underlined blue text. The PAM sequence is indicated by the underlined red text and in-frame ATG is indicated in green. (B) The DNA sequence of two alleles of cells genetically edited with the CRISPR/Cas9 system. The black arrows indicate the deleted sites. (C) DNA sequence analysis of two alleles showing the *PTEN* mutation. The black arrows indicate the deleted site. The WT sequence is from the parental cell line. PAM, protospacer adjacent motif; WT, wildtype; *PTEN*, phosphatase and tensin homolog; CRISPR/Cas9, clustered regularly interspaced short palindromic repeats/CRISPR-associated protein;  $\Delta$ *PTEN*, *PTEN*-knockout cell line.

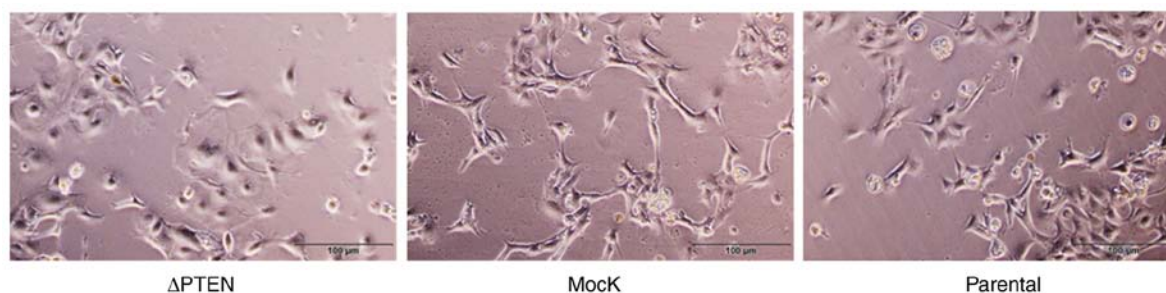


Figure 2. Photomicrograph depicting cell morphology in  $\Delta$ *PTEN*, mock and parental cell lines. *PTEN*, phosphatase and tensin homolog;  $\Delta$ *PTEN*, *PTEN*-knockout cell line.

(SAS Institute Inc; Tokyo, Japan).  $P < 0.05$  was considered to indicate a statistically significant difference ( $^*P < 0.05$ ;  $^{**}P < 0.01$ ;  $^{***}P < 0.001$ ).

## Results

**Establishment of *PTEN*-knockout cells using the CRISPR/Cas9 System.** The present study performed genome editing (targeting sequence presented in Fig. 1A) using the CRISPR/Cas9 system

and obtained multiple clones ( $\Delta$ *PTEN*). Fig. 1B and C reveal DNA sequencing of target sites in the resultant clones. These results demonstrated that targeting *PTEN* with the CRISPR/Cas9 system effectively generated mutant-*PTEN* clones. Next, the present study assessed the effects of *PTEN* inactivation in the resulting clones. Overall, the general appearance was similar between parental, mock, and  $\Delta$ *PTEN* cells; however, marginal differences were observed in the morphological appearance of  $\Delta$ *PTEN* cells such as heterogeneity of the cell shape (Fig. 2).

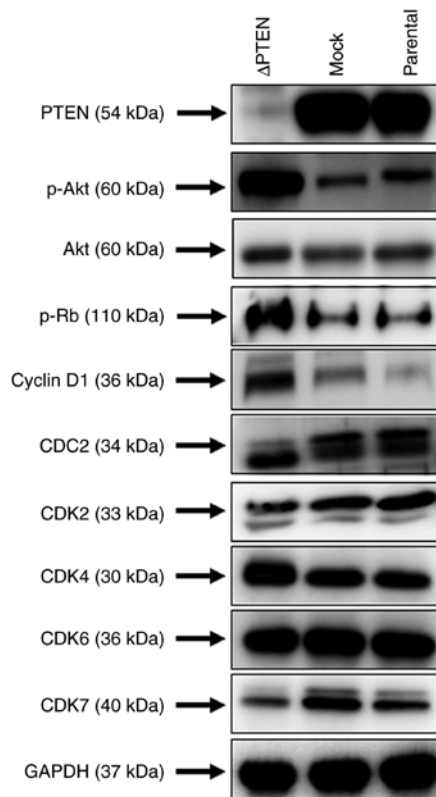


Figure 3. Western blot analysis of  $\Delta$ PTEN cells. Immunoblots showing protein expression of basal PTEN, phospho-Akt, and the cell cycle-related proteins pRb, Cyclin D1, CDC2, CDK2, CDK4, CDK6, and CDK7 in  $\Delta$ PTEN, mock and parental cell lines. GAPDH was used as a loading control. PTEN, phosphatase and tensin homolog;  $\Delta$ PTEN, PTEN-knockout cell line; CDK, cyclin dependent kinase; CDC2, cyclin-dependent protein kinase 1; p, phosphorylated; Akt, RAC-alpha serine/threonine-protein kinase; Rb, retinoblastoma tumor-suppressor protein.

Using western blot analysis, the present study verified the effective knockout of PTEN in  $\Delta$ PTEN cells. Fig. 3 shows that the expression of PTEN was present in the parental strain and mock-transfected cells but was effectively downregulated in  $\Delta$ PTEN cells. Accordingly, Akt phosphorylation levels increased in the absence of PTEN. Activation of the PI3K/Akt pathway promotes the cellular proliferation of transformed cells; thus, the expression of molecules involved in proliferation was then assessed. In  $\Delta$ PTEN cells, the upregulation of Akt phosphorylation was associated with the elevated expression of cyclin D1, cyclin dependent kinase (CDK)4, and decreased expression of CDK7. In addition, increased phosphorylation of the retinoblastoma tumor-suppressor protein (RB) was observed, a known regulator of cellular proliferation, in  $\Delta$ PTEN cells. As the expression of molecules involved in the cell cycle was demonstrated to be enhanced in  $\Delta$ PTEN cells, the present study then assessed the effects of PTEN inactivation on cell viability. Fig. 4 shows that the inactivation of the PTEN function in  $\Delta$ PTEN cells results in increased cell growth and enhanced colony formation.

**Microarray and miRNA array analysis of PTEN-knockout cells.** Using gene microarrays, the present study assessed changes in gene expression following the loss of the PTEN function and focused on genes that were differentially expressed in  $\Delta$ PTEN cells relative to mock-transfected cells and the parental strain (Fig. 5). Overall, 111 genes were

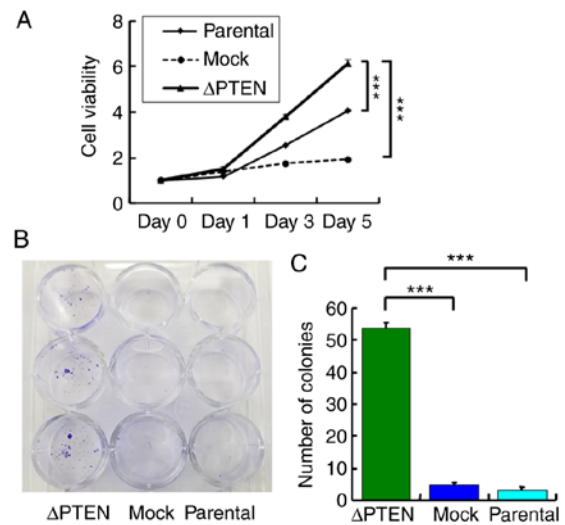


Figure 4. PTEN-knockout enhances cell viability and colony formation. (A) MTT analysis of growth curves of  $\Delta$ PTEN, mock and parental cells. The optical density (550 nm) at each time point (day 0, 1, 3, 5 and 7) is presented as the mean  $\pm$  standard error of the mean (n=6). (B) A colony formation assay was performed by seeding 500 cells into six-well plates. After 14 days, the cells were stained with crystal violet and imaged. (C) Representative micrographs and quantification of colonies. Values are presented as the mean  $\pm$  standard error of the mean (n=3). \*\*\*P<0.001. PTEN, phosphatase and tensin homolog;  $\Delta$ PTEN, PTEN-knockout cell line.

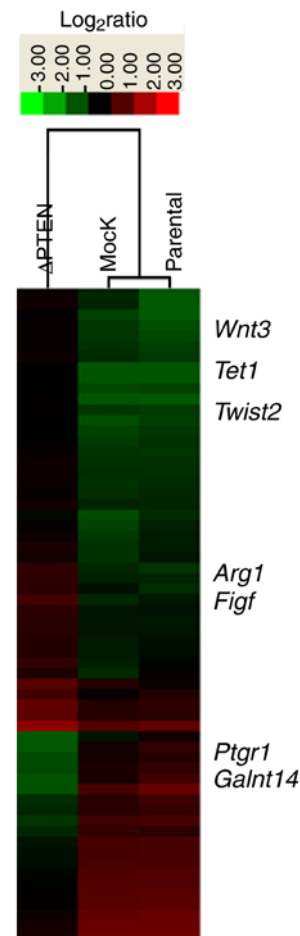


Figure 5. Microarray analysis identification of novel genes associated with PTEN expression. Heat map representing gene expression changes (at least 10-fold) in  $\Delta$ PTEN, mock, and parental cells. PTEN, phosphatase and tensin homolog;  $\Delta$ PTEN, PTEN-knockout cell line; Tet1, Tet methylcytosine dioxygenase 1; Figf, C-fos-induced growth factor; Twist2, twist family BHLH transcription factor 2; Arg1, Arginase 1; Ptgr1, prostaglandin reductase 1; Galnt14, polypeptide N-acetylgalactosaminyltransferase 14.

Table II. Genes that are upregulated 10-fold or more in phosphatase and tensin homolog knockout cells.

Gene symbol	Accession	UniGene	Function	Relative intensity of KO/mock
Sprr2d	NM_011470	Mm.87820	Small proline-rich protein 2D	74
Serp1nb6b	NM_011454	Mm.36526	Serine (or cysteine) peptidase inhibitor, clade B, member 6b	36
Lifr	NM_013584	Mm.149720	Leukemia inhibitory factor receptor	36
Tet1	NM_001253857	Mm.491965	Tet methylcytosine dioxygenase 1	32
Sprr2e	NM_011471	Mm.261596	Small proline-rich protein 2E	29
Dppa2	NM_028615	Mm.27857	Developmental pluripotency associated 2	29
BB612626	BB612626	Mm.463155	Not indicated	26
Gap43	NM_008083	Mm.1222	Growth associated protein 43	25
Sprr1b	NM_009265	Mm.140151	Small proline-rich protein 1B	23
Tspan10	NM_145363	Mm.209875	Tetraspanin 10	21
Tex15	NM_031374	Mm.280624	Testis expressed gene 15	20
Prl7a2	NM_011168	Mm.153999	Prolactin family 7, subfamily a, member 2	19
Gm9519	XR_391191	Mm.389803	Not indicated	19
Nlrc5	NM_001033207	Mm.334720	NLR family, CARD domain containing 5	19
Gm26579	XR_380816	Mm.356554	Not indicated	19
Aqp9	NM_001271843	Mm.335570	Aquaporin 9	18
Sp110	NM_175397	Mm.335802	Sp110 nuclear body protein	18
Gm29824	XR_870586	Mm.135986	ncRNA	17
Sdr16c6	BC125450	Mm.298546	Short chain dehydrogenase/reductase family 16C, member 6	17
Prl7a1	NM_008930	Mm.196424	Prolactin family 7, subfamily a, member 1	17
Cfhr2	NM_001025575	Mm.439660	Complement factor H-related 2	17
Fa2h	NM_178086	Mm.41083	Fatty acid 2-hydroxylase	17
Zfp352	NM_153102	Mm.214642	Zinc finger protein 352	16
Cyp7a1	NM_007824	Mm.57029	Cytochrome P450, family 7, subfamily a, polypeptide 1	16
Tvp23a	NM_001013778	Mm.325732	Trans-golgi network vesicle protein 23A	15
Mmell1	NM_013783	Mm.116944	Membrane metallo-endopeptidase-like 1	15
Ivl	NM_008412	Mm.207365	Involucrin	15
Sprr2h	NM_011474	Mm.10693	Small proline-rich protein 2H	15
AV154423	AV154423	Mm.486971	Not indicated	15
Phf11d	NM_199015	Mm.479285	PHD finger protein 11D	15
Col8a1	NM_007739	Mm.130388	Collagen, type VIII, alpha 1	14
Evi2a	NM_001033711	Mm.439665	Ecotropic viral integration site 2a	14
Samd15	NM_001290288	Mm.302304	Sterile alpha motif domain containing 15	14
Gm13119	NM_001034101	Mm.389596	Not indicated	14
Trp63	NM_011641	Mm.20894	Transformation related protein 63	14
AA623943	XM_006534607	not indicated	Expressed sequence AA623943	14
Defb3	NM_013756	Mm.103651	Defensin beta 3	14
Gm30692	XR_863174	not indicated	ncRNA	14
Gm32204	XM_006497575	not indicated	Not indicated	14
Serp1nb2	NM_011111	Mm.271870	Serine (or cysteine) peptidase inhibitor, clade B, member 2	14
Rsad2	NM_021384	Mm.24045	Radical S-adenosyl methionine domain containing 2	14
Gm31115	XR_390648	not indicated	Not indicated	14
Slco4a1	NM_148933	Mm.133687	Solute carrier organic anion transporter family, member 4a1	14
Sod3	NM_011435	Mm.2407	Superoxide dismutase 3, extracellular	13
Ccdc153	NM_001081369	Mm.347681	Coiled-coil domain containing 153	13

Table II. Continued

Gene symbol	Accession	UniGene	Function	Relative intensity of KO/mock
Lce1d	NM_027137	Mm.176243	Late cornified envelope 1D	13
Twist2	NM_007855	Mm.9474	Twist basic helix-loop-helix transcription factor 2	13
Plcb1	NM_019677	Mm.330607	Phospholipase C, beta 1	13
Olf376	NM_001172686	Mm.236410	Olfactory receptor 376	13
Gm19619	NR_040428	Mm.125059	Not indicated	13
Dnm3	NM_172646	Mm.441620	Dynamin 3	13
Chst5	NM_019950	Mm.432506	Carbohydrate (N-acetylglucosamine 6-O) sulfotransferase 5	13
BF119155	BF119155	Mm.432156	Not indicated	12
Arg1	NM_007482	Mm.154144	Arginase, liver	12
Cdh7	AK034096	Mm.487119	Cadherin 7, type 2	12
Ugt1a6b	NM_201410	Mm.300095	UDP glucuronosyltransferase 1 family, polypeptide A6B	12
Chrna5	NM_176844	Mm.103778	Cholinergic receptor, nicotinic, alpha polypeptide 5	12
Phf11a	NM_172603	Mm.254918	PHD finger protein 11A	12
Sh3tc2	NM_172628	Mm.262320	SH3 domain and tetratricopeptide repeats 2	12
Armc2	NM_001034858	Mm.211320	Armadillo repeat containing 2	12
Fgf21	NM_020013	Mm.143736	Fibroblast growth factor 21	12
Ccdc109b	NM_025779	Mm.31056	Coiled-coil domain containing 109B	12
Klk7	NM_011872	Mm.251227	Kallikrein related-peptidase 7 (chymotryptic, stratum corneum)	12
Sh3gl3	NM_017400	Mm.432002	SH3-domain GRB2-like 3	11
Gm17202	XR_389494	not indicated	Not indicated	11
Iigp1	NM_021792	Mm.261140	Interferon inducible GTPase 1	11
AF067061	NM_199060	Mm.247428	cDNA sequence AF067061	11
Plce1	NM_019588	Mm.34031	Phospholipase C, epsilon 1	11
Tprg	NM_175165	Mm.126851	Transformation related protein 63 regulated	11
Spint3	NM_001177401	Mm.234248	Serine peptidase inhibitor, Kunitz type, 3	11
LOC102634459	XR_387206	not indicated	Not indicated	11
Gm4340	NM_001177535	Mm.339215	Not indicated	11
Arhgap9	NM_001285785	Mm.227198	Rho GTPase activating protein 9	11
Aldh1a3	NM_053080	Mm.140988	Aldehyde dehydrogenase family 1, subfamily A3	11
Adh7	NM_009626	Mm.8473	Alcohol dehydrogenase 7 (class IV), mu or sigma polypeptide	11
Prl3d2	NM_172155	Mm.458451	Prolactin family 3, subfamily d, member 1	11
Lama1	AK051116	Mm.303386	Laminin, alpha 1	11
Gm7978	NM_001270457	Mm.380154	Not indicated	11
BB114814	XM_006508432	Mm.304207	Expressed sequence BB114814	11
D5Erd577e	NM_177187	Mm.348793	DNA segment, Chr 5, ERATO Doi 577, expressed	11
Lrrn4	NM_177303	Mm.386903	Leucine rich repeat neuronal 4	11
Trav12-1	BC038136	Mm.333502	T cell receptor alpha variable 12-1	11
CV783874	CV783874	Mm.441595	Not indicated	11
Igfbp5	NM_010518	Mm.405761	Insulin-like growth factor binding protein 5	11
Gm3259	NM_001270456	Mm.402477	Not indicated	10
Gm4665	AK132957	Mm.437523	Not indicated	10
Sox11	NM_009234	Mm.41702	SRY (sex determining region Y)-box 11	10
Tctv1	NM_018756	Mm.302175	2-Cell-stage, variable group, member 1	10
Sprr3	NM_011478	Mm.57092	Small proline-rich protein 3	10
Podn	NM_001285956	Mm.74710	Podocan	10
Ifit3b	NM_001005858	Mm.271850	Interferon-induced protein with tetratricopeptide repeats 3B	10

Table II. Continued

Gene symbol	Accession	UniGene	Function	Relative intensity of KO/mock
Gabra1	NM_010250	Mm.439668	Gamma-aminobutyric acid (GABA) 1 A receptor, subunit alpha	10
Ifi44	NM_133871	Mm.30756	Interferon-induced protein 44	10
a	NM_015770	Mm.315593	Nonagouti	10
Rd31	XM_006515764	Mm.134213	Retinal degeneration 3-like	10
Figf	NM_010216	Mm.297978	Vascular endothelial growth factor D	10
B430212C06Rik	NR_033214	Mm.491997	Not indicated	10
AK034098	AK034098	Mm.446266	Not indicated	10
Bank1	NM_001033350	Mm.30832	B cell scaffold protein with ankyrin repeats 1	10
Sel1l3	NM_172710	Mm.235020	Sel-1 suppressor of lin-12-like 3	10
Sgsm1	NM_172718	Mm.200203	Small G protein signaling modulator 1	10
Krt13	NM_010662	Mm.4646	Keratin 13	10
Tpo	NM_009417	Mm.4991	Thyroid peroxidase	10
Tnfrsf18	NM_009400	Mm.491989	Tumor necrosis factor receptor superfamily, member 18	10
Klra2	NM_008462	Mm.4783	Killer cell lectin-like receptor, subfamily A, member 2	10
Pcdh7	NM_018764	Mm.332387	Protocadherin 7	10
Cbr2	NM_007621	Mm.21454	Carbonyl reductase 2	10
Wnt3	NM_009521	Mm.159091	Wingless-type MMTV integration site family, member 3	10
AK042637	AK042637	not indicated	Not indicated	10
CO811058	CO811058	Mm.421039	Not indicated	10
St18	NM_173868	Mm.234612	Suppression of tumorigenicity 18	10

Table III. Genes that are downregulated 10-fold or more in phosphatase and tensin homolog knockout cells.

Gene symbol	Accession	UniGene	Function	Relative intensity of mock/KO
Wtip	NM_207212	Mm.422738	WT1-interacting protein	139
Gm32139	XR_001782443	not indicated	not indicated	38
Gm38426	NR_103491	Mm.437155	not indicated	37
Ptgr1	NM_025968	Mm.34497	prostaglandin reductase	30
Pla2g16	NM_139269	Mm.274810	phospholipase A2, group XVI	29
Galnt14	NM_027864	Mm.271953	UDP-N-acetyl-alpha-D-galactosamine:polypeptide N-acetylgalactosaminyltransferase 14	19
Dhrs4	NM_030686	Mm.27427	dehydrogenase/reductase (SDR family) member 4	19
Fam124a	NM_001243857	Mm.291864	family with sequence similarity 124, member A	18
Robo1	NM_019413	Mm.310772	roundabout guidance receptor 1	16
Evc2	NM_145920	Mm.25506	Ellis van Creveld syndrome 2	15
Spats2l	NM_144882	Mm.159989	spermatogenesis associated, serine-rich 2-like	14
Ttc12	NM_172770	Mm.177413	tetratricopeptide repeat domain 12	14
Gxylt2	NM_198612	Mm.272037	glucoside xylosyltransferase 2	14
Tmem173	NM_028261	Mm.45995	transmembrane protein 173	13
Gm2030	NM_001100445	Mm.411645	not indicated	13
Gm16404	NM_001220497	Mm.380174	not indicated	13
Gm1993	NM_001102677	Mm.484626	not indicated	12
Gm10487	NM_001100609	Mm.483167	not indicated	12
Gm5168	NM_001025607	Mm.370361	not indicated	12
Slx	NM_001136476	Mm.489202	Sycp3 like X-linked	12
Scml2	NM_001290651	Mm.159173	sex comb on midleg-like 2	11
Gm14625	NM_001220498	Mm.477978	not indicated	11
Ppic	NM_008908	Mm.4587	peptidylprolyl isomerase C	10

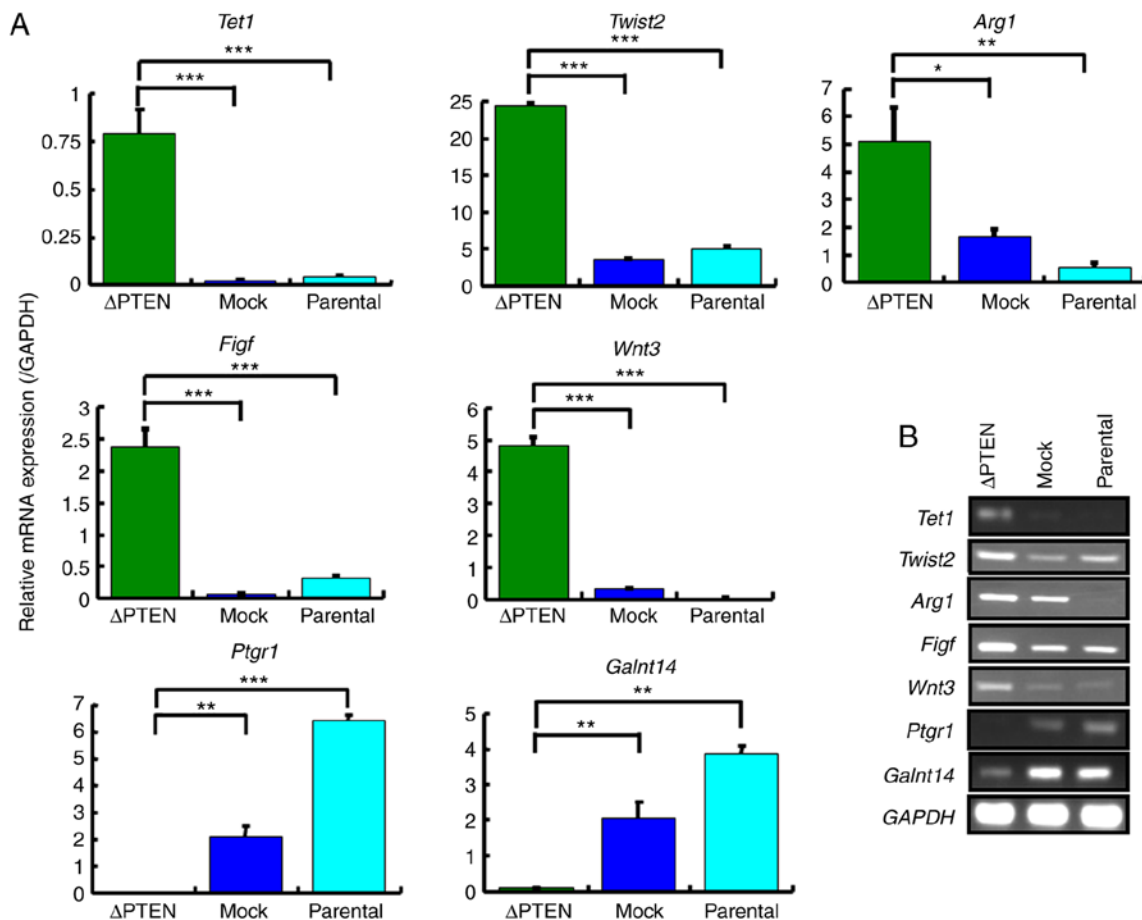


Figure 6. Confirmation of mRNA expression levels in selected genes with a  $\geq 10$ -fold change in the microarray analysis. (A) Expression levels of *Tet1*, *Twist2*, *Arg1*, *Figf*, *Wnt3*, *Ptgr1*, and *Galnt14* in  $\Delta$ PTEN, mock, and parental cell lines were analyzed using the qRT-PCR method. The relative gene expression levels are shown after normalization to GAPDH mRNA expression. (B) RT-PCR analysis of the mRNA expression of *Tet1*, *Twist2*, *Arg1*, *Figf*, *Wnt3*, *Ptgr1* and *Galnt14* in  $\Delta$ PTEN, mock, and parental cell lines. \* $P < 0.05$ ; \*\* $P < 0.01$ ; \*\*\* $P < 0.001$ . PTEN, phosphatase and tensin homolog;  $\Delta$ PTEN, PTEN-knockout cell line; *Tet1*, Tet methylcytosine dioxygenase 1; *Figf*, C-fos-induced growth factor; *Twist2* twist family BHLH transcription factor 2; *Arg1*, Arginase 1; *Ptgr1*, prostaglandin reductase 1; *Galnt14*, polypeptide N-acetylgalactosaminyltransferase 14; qRT-PCR, quantitative reverse transcription- polymerase chain reaction.

upregulated by at least 10-fold, including one with a 74-fold increase in  $\Delta$ PTEN cells (Table II). In addition, 23 genes were identified to be substantially downregulated by  $\geq 10$ -fold, one with a 139-fold decrease (Table III).

The mRNA expression levels of *Tet1*, *Twist2*, *Arg1*, *Figf*, *Wnt3*, *Ptgr1*, and *Galnt14* were measured by RT-qPCR to confirm the results of the microarray analysis (Fig. 6A). The expression patterns of the RT-PCR analysis were parallel to those in the microarray, thereby verifying the results (Fig. 6B).

Next, the present study performed gene enrichment profiling to gain better insight into the genes differentially expressed after PTEN-knockout in the model. The analysis using the Panther annotation database revealed that 64 of the 111 upregulated genes corresponded to 15 pathways (Fig. 7).

Furthermore, the expression of non-coding RNAs, in particular miRNAs, were assessed to further delve into the impact of PTEN inactivation and altered gene expression. Notably, the miRNA expression analysis in this study revealed that only the mmu-miR-210-3p expression increased ( $\geq 10$ -fold) due to PTEN-knockout. Corroborating our initial observation, the RT-qPCR analysis presented an evident increase of mmu-miR-210-3p in  $\Delta$ PTEN cells compared with the parental strain and mock-transfected cells (Fig. 8).

## Discussion

The present study investigated the changes in carcinogenesis-associated genes caused by PTEN deficiency in a mouse prostate cancer model. A PTEN-deficient mouse prostate cancer isogenic cell line was established using the CRISPR/Cas9 system. The phosphorylation of Akt and the expression of cyclin D1 were elevated in PTEN-deficient cells. Although the expression of CDK7 was revealed to be decreased, the reason remains unknown. The expression levels of cyclinD1 and CDK4 that increased as demonstrated by western blotting, were not recognized as much different from that of parental cell or mock cell in microarray analysis. The reason for this increase in the expression currently remains unclear. Furthermore, microarray and miRNA arrays were used to assess the changes in gene expression. These results suggested that the PTEN expression is essential for normal gene expression.

The present study observed alterations in the expression levels of various genes due to the loss of the PTEN gene, which may be attributed to an increase in the expression of TET1. Demethylation is increased in several genes due to the enhanced expression of TET1, a dioxygenase that catalyzes the conversion of the modified genomic base 5-methylcytosine (5 mc)

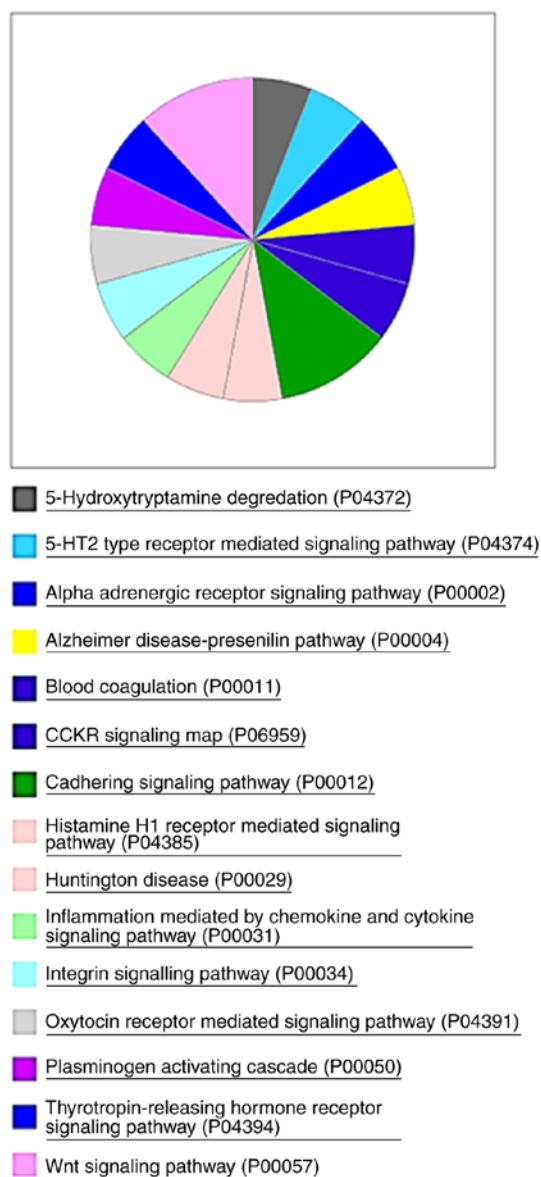


Figure 7. Biological processes and pathways altered in  $\Delta$ PTEN cells. Panther gene ontology enrichment pie chart of genes upregulated after PTEN knockout. PTEN, phosphatase and tensin homolog;  $\Delta$ PTEN, PTEN-knockout cell line.

into 5-hydroxymethylcytosine (5hmc). Reportedly, Nanog is an example of a gene induced by Tet1 expression. Not only does Nanog have a role in the maintenance of mouse ES cells (20), but also in the maintenance of cancer stem cells, suppression of apoptosis, promotion of cancer progression and metastasis, and angiogenesis (21). These findings suggest that PTEN deficiency drives TET1 and TET1-gene regulation during carcinogenesis; however, the underlying reasons for an increase in the TET1 expression in PTEN deficiency remain unclear.

In this model, we established the upregulation of *Twist2*, *Figf*, *Wnt3*, and *Arg1* in response to *Pten*-knockout; these genes play vital roles in the development and progression of cancer and promote the immune suppression in the surrounding tumor microenvironment.

*Twist2*, a member of the basic helix-loop-helix (BHLH) transcription factors, is overexpressed in several cancer types.

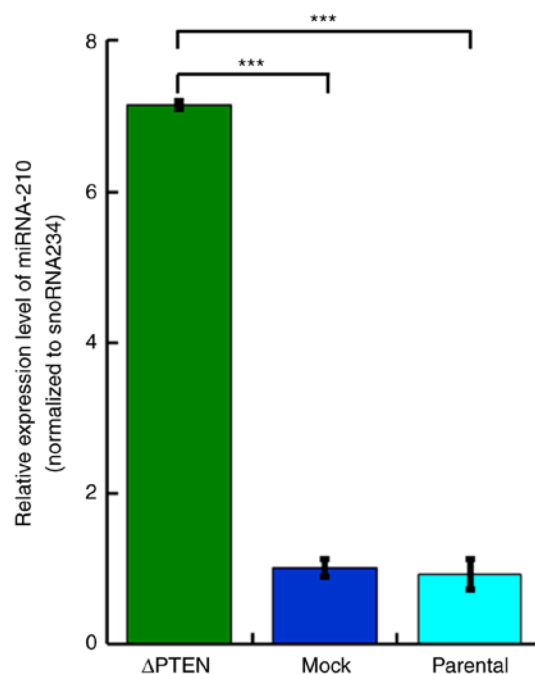


Figure 8. Analysis of miR-210 expression levels in  $\Delta$ PTEN, mock and parental cell lines using reverse transcription-quantitative polymerase chain reaction. Results are normalized to snoRNA234 expression. \*\*\*P<0.001. PTEN, phosphatase and tensin homolog;  $\Delta$ PTEN, PTEN-knockout cell line.

Previously, studies have reported the correlation of Twist expression with head and neck squamous cell carcinomas, cervical carcinomas, and ovarian cancer (22-24). Yang *et al* reported that hypoxia inducible factor-1 (HIF-1) promotes EMT through direct regulation of Twist expression (25). Twist is a master regulator of gastrulation and mesoderm specification and is implicated to be essential in the mediation of cancer metastasis (25). In this study, the expression of Twist was enhanced by the absence of functional PTEN, suggesting transcriptional regulation by mechanisms mediated by proteins other than HIF-1.

Figf, also termed vascular endothelial growth factor (VEGF)-D is a member of the platelet-derived growth factor (PDGF)/VEGF family and is active in angiogenesis and endothelial cell growth. Reportedly, the normal VEGF-D expression is detected in the lung, heart, skeletal muscle, skin, adrenal gland, and gastrointestinal tract (26-28). In addition, VEGF-D is upregulated in glioblastoma (29), melanoma (30), colorectal carcinoma (31), breast carcinoma (32), and cervical intraepithelial neoplasia (33). Tian *et al* reported that PTEN suppresses VEGF expression in HCC through both phosphatase-dependent and -independent mechanisms (34). The present study also implicated that PTEN regulates VEGF expression through both phosphatase- and HIF-1 $\alpha$ -independent mechanisms. Kaushal *et al* (35) reported that VEGF-D expression is observed in all prostate cancer tissues and that it is increased in samples at advanced stages compared with those at the early stage; however, they did not report the correlation between VEGF-D expression and PTEN. In 20% of prostate cancers, PTEN is deleted (36). PTEN-deficient prostate cancers express VEGF-D at an early stage; therefore, it is imperative to compare the expression between tumors with and without PTEN.

The Wingless-type MMTV integration site family genes comprise structurally related genes that encode a secreted

signaling protein implicated in oncogenesis and several developmental processes, including the regulation of cell fate and patterning during embryogenesis (37,38). In normal tissues, *Wnt3* RNA is primarily detected in the testis, skin, and brain. Reportedly, *Wnt3* is associated with cancer progression, invasion, and malignant conversion in cancer of the gastric (39), lungs (40,41), and hepatocellular carcinoma (42,43). In  $\Delta$ PTEN cells, the cyclin D1 expression was upregulated. In addition, PTEN loss has been reported to augment cyclin D1 expression, although the underlying mechanism remains only partially understood. However, Zang *et al* reported that the Wnt/b-catenin pathway stimulates increased cyclin D1 levels in lymph node metastasis in papillary thyroid cancer (44). These results suggest an association between the PTEN-loss-induced *Wnt3* expression and the subsequent upregulation of cyclin D1.

In mammals, two arginase isoforms (Arg1 and Arg2) have been identified. Arg1 is known as the liver type and is expressed in hepatocytes (45). In mice, Arg1 can also be expressed in myeloid cells under the stimulation of T helper 2 cytokines interleukin (IL)-4 and IL-13 (46), transforming growth factor- $\beta$  (47), macrophage-stimulating protein (48), or GM-CSF (49). Although immune responses are controlled by amino acid metabolism, Rodriguez *et al* reported that arginase produced by tumor-infiltrating macrophages repressed the expression of the T-cell receptor CD3z, resulting in the suppression of antigen-specific T-cell responses (46). In this study, it was observed that Arg1 expression increased following Pten deficiency; however, to the best of the author's knowledge, there are no reports demonstrating that Arg1 is highly expressed in any cancer other than liver cancer. Recent cancer treatment strategies have targeted arginine metabolism (50,51), thereby making Arg1 an attractive therapeutic approach for PTEN-deficient tumors.

The present study also analyzed differential expression of miRNA and observed an increased expression of mmu-miR-210-3p in the PTEN-deficient cell line. Reportedly, the expression of miR-210 is induced by HIF-1, which is known to be upregulated in PTEN-deficient cells (52). The expression levels of the target genes of miR-210 were not observed to be altered in the present study. Studies have suggested that miR-210 is involved in multiple processes, including angiogenesis, metastasis, oncogenesis, decreased cell division, and tumor suppression (53,54). However, the exact function remains unclear and requires further investigation.

In conclusion, the present study established a mouse prostate cancer cell model of PTEN deficiency and provided evidence of altered expression of genes associated with the deregulation of signaling processes implicated in human cancers. Gene expression profiling suggested enhanced regulation cancer hallmarks, including cell proliferation, angiogenesis, metastasis, and immunosuppression. However, further studies are warranted to dissect and elucidate molecular mechanisms involved in promoting PTEN-deficient cancer progression.

#### Acknowledgements

Not applicable.

#### Funding

No funding was received.

#### Availability of data and materials

The datasets used during the present study are available from the corresponding author upon reasonable request.

#### Authors' contributions

AT, KY, SK, AO, HU, MADV, YK, SS, RU, TN and YH equally took part in the conception and design of the study, acquisition and interpretation of data, drafting the article and final approval of the version to be published.

#### Ethics approval and consent to participate

Not applicable.

#### Patient consent for publication

Not applicable.

#### Competing interests

The authors state that they have no competing interests.

#### References

1. Toker A and Cantley LC: Signalling through the lipid products of phosphoinositide-3-OH kinase. *Nature* 12: 673-676, 1997.
2. Li J, Yen C, Liaw D, Podsypanina K, Bose S, Wang SI, Puc J, Miliareis C, Rodgers L, McCombie R, *et al*: *PTEN*, a putative protein tyrosine phosphatase gene mutated in human brain, breast, and prostate cancer. *Science* 28: 1943-1947, 1997.
3. Steck PA, Pershouse MA, Jasser SA, Yung WK, Lin H, Ligon AH, Langford LA, Baumgard ML, Hattier T, Davis T, *et al*: Identification of a candidate tumour suppressor gene, *MMAC1*, at chromosome 10q23.3 that is mutated in multiple advanced cancers. *Nat.Genet* 15: 356-362, 1997.
4. Tamura M, Gu J, Matsumoto K, Aota S, Parsons R, and Yamada KM: Inhibition of cell migration, spreading, and focal adhesions by tumor suppressor PTEN. *Science* 280: 1614-1617, 1998.
5. Yamada KM and Araki M: Tumor suppressor PTEN: Modulator of cell signaling, growth, migration, and apoptosis. *J Cell Sci* 114: 2375-2382, 2001.
6. Waite KA and Eng C: Protean PTEN: Form and function. *Am J Hum Genet* 70: 829-844, 2002.
7. McCall P, Witton CJ, Grimsley S, Nielsen KV and Edwards J: Is PTEN loss associated with clinical outcome measures in human prostate cancer? *Br J Cancer* 99: 1296-1301, 2008.
8. Davies MA: Regulation, role, and targeting of Akt in cancer. *J Clin Oncol* 29: 4715-4717, 2011.
9. Carnero A and Paramio JM: The PTEN/PI3K/AKT pathway in vivo, cancer mouse models. *Front Oncol* 4: 252, 2014.
10. De Velasco MA, Tanaka M, Yamamoto Y, Hatanaka Y, Koike H, Nishio K, Yoshikawa K and Uemura H: Androgen deprivation induces phenotypic plasticity and promotes resistance to molecular targeted therapy in a *PTEN*-deficient mouse model of prostate cancer. *Carcinogenesis* 35: 2142-2153, 2014.
11. Yamamoto Y, De Velasco MA, Kura Y, Nozawa M, Hatanaka Y, Oki T, Ozeki T, Shimizu N, Minami T, Yoshimura K, *et al*: Evaluation of in vivo responses of sorafenib therapy in a preclinical mouse model of *PTEN*-deficient of prostate cancer. *J Transl Med* 8: 150, 2015.
12. Koike H, Nozawa M, De Velasco MA, Kura Y, Ando N, Fukushima E, Yamamoto Y, Hatanaka Y, Yoshikawa K, Nishio K and Uemura H: Conditional *PTEN*-deficient mice as a prostate cancer chemoprevention model. *Asian Pac J Cancer Prev* 16: 1827-1831, 2015.
13. De Velasco MA, Kura Y, Yoshikawa K, Nishio K, Davies BR and Uemura H: Efficacy of targeted AKT inhibition in genetically engineered mouse models of *PTEN*-deficient prostate cancer. *Oncotarget* 29: 15959-15976, 2016.

14. Jia L, Ji S, Maillet JC and Zhang X: PTEN suppression promotes neurite development exclusively in differentiating PC12 cells via PI3-kinase and MAP kinase signaling. *J Cell Biochem* 111: 1390-1400, 2010.
15. Khan FA, Pandupuspitasari NS, Chun-Jie H, Ao Z, Jamal M, Zohaib A, Khan FA, Hakim MR and Shujun Z: CRISPR/Cas9 therapeutics: A cure for cancer and other genetic diseases. *Oncotarget* 7: 52541-52552, 2016.
16. Ran FA, Hsu PD, Wright J, Agarwala V, Scott DA and Zhang F: Genome engineering using the CRISPR-Cas9 system. *Nat Protoc* 8: 2281-2308, 2013.
17. Mizuno S, Hanamura I, Ota A, Karnan S, Narita T, Ri M, Mizutani M, Goto M, Gotou M, Tsunekawa N, *et al*: Overexpression of salivary-type amylase reduces the sensitivity to bortezomib in multiple myeloma cells. *Int J Hematol* 102: 569-578, 2015.
18. Mi H, Huang X, Muruganujan A, Tang H, Mills C, Kang D and Thomas PD: PANTHER version 11: Expanded annotation data from Gene Ontology and Reactome pathways, and data analysis tool enhancements. *Nucleic Acids Res* 45: D183-D189, 2017.
19. Livak KJ and Schmittgen TD: Analysis of relative gene expression data using real-time quantitative PCR and the  $2^{-\Delta\Delta CT}$  method. *Methods* 25: 402-408, 2001.
20. Ito S, D'Alessio AC, Taranova OV, Hong K, Sowers LC and Zhang Y: Role of Tet proteins in 5mC to 5hmC conversion, ES cell self renewal and inner cell mass specification. *Nature* 26: 1129-1133, 2010.
21. Gawlik-Rzemieniewska N and Bednarek I: The role of NANOG transcriptional factor in the development of malignant phenotype of cancer cells. *Cancer Biol Ther* 17: 1-10, 2016.
22. Gasparotto D, Polesel J, Marzotto A, Colladel R, Piccinin S, Modena P, Grizzo A, Sulfaro S, Serraino D, Barzan L, *et al*: Overexpression of TWIST2 correlates with poor prognosis in head and neck squamous cell carcinomas. *Oncotarget* 2: 1165-1175, 2011.
23. Li Y, Wang W, Wang W, Yang R, Wang T, Su T, Weng D, Tao T, Li W, Ma D, *et al*: Correlation of TWIST2 up-regulation and epithelial-mesenchymal transition during tumorigenesis and progression of cervical carcinoma. *Gynecol Oncol* 124: 112-118, 2012.
24. Mao Y, Xu J, Song G and Yin H: Twist2 promotes ovarian cancer cell survival through activation of Akt. *Oncol Lett* 6: 169-174, 2013.
25. Yang MH, Wu MZ, Chiou SH, Chen PM, Chang SY, Liu CJ, Teng SC and Wu KJ: Direct regulation of TWIST by HIF-1 $\alpha$  promotes metastasis. *Nat Cell Biol* 10: 295-305, 2008.
26. Yamada Y, Nezu J, Shimane M and Hirata Y: Molecular cloning of a novel vascular endothelial growth factor, VEGF-D. *Genomics* 42: 483-488, 1997.
27. Achen MG, Jeltsch M, Kukk E, Mäkinen T, Vitali A, Wilks AF, Alitalo K and Stacker SA: Vascular endothelial growth factor D (VEGF-D) is a ligand for the tyrosine kinases VEGF receptor 2 (Flk1) and VEGF receptor 3 (Flt4). *Proc Natl Acad Sci USA* 95: 548-553, 1998.
28. Trompezinski S, Berthier-Vergnes O, Denis A, Schmitt D and Viac J: Comparative expression of vascular endothelial growth factor family members, VEGF-B, -C and -D, by normal human keratinocytes and fibroblasts. *Exp Dermatol* 13: 198-105, 2004.
29. Debinski W, Slagle-Webb B, Achen MG, Stacker SA, Tulchinsky E, Gillespie GY and Gibo DM: VEGF-D is an X-linked/AP-1 regulated putative onco-angiogen in human glioblastoma multiforme. *Mol Med* 7: 598-608, 2001.
30. Achen MG, Williams RA, Minekus MP, Thornton GE, Stenvers K, Rogers PA, Lederman F, Roufail S and Stacker SA: Localization of vascular endothelial growth factor-D in malignant melanoma suggests a role in tumour angiogenesis. *J Pathol* 193: 147-154, 2001.
31. White JD, Hewett PW, Kosuge D, McCulloch T, Enholm BC, Carmichael J and Murray JC: Vascular endothelial growth factor-D expression is an independent prognostic marker for survival in colorectal carcinoma. *Cancer Res* 62: 1669-1675, 2002.
32. Nakamura Y, Yasuoka H, Tsujimoto M, Yang Q, Imabun S, Nakahara M, Nakao K, Nakamura M, Mori I and Kakudo K: Prognostic significance of vascular endothelial growth factor D in breast carcinoma with longterm follow-up. *Clin Cancer Res* 9: 716-721, 2003.
33. Van Trappen PO, Steele D, Lowe DG, Baithun S, Beasley N, Thiele W, Weich H, Krishnan J, Shepherd JH, Pepper MS, *et al*: Expression of vascular endothelial growth factor (VEGF)-C and VEGF-D, and their receptor VEGFR-3, during different stages of cervical carcinogenesis. *J Pathol* 201: 544-554, 2003.
34. Tian T, Nan KJ, Wang SH, Liang X, Lu CX, Guo H, Wang W and Ruan ZP: PTEN regulates angiogenesis and VEGF expression through phosphatase-dependent and -independent mechanisms in HepG2 cells. *Carcinogenesis* 31: 1211-1219, 2010.
35. Kaushal V, Mukunyadzi P, Dennis RA, Siegel ER, Johnson DE and Kohli M: Stage-specific characterization of the vascular endothelial growth factor axis in prostate cancer: Expression of lymphangiogenic markers is associated with advanced-stage disease. *Clin Cancer Res* 11: 584-593, 2005.
36. Netto GJ: Molecular updates in prostate cancer. *Surg Pathol* 8: 561-580, 2015.
37. Clevers H: Wnt/beta-catenin signaling in development and disease. *Cell* 127: 469-480, 2006.
38. He S, Lu Y, Liu X, Huang X, Keller ET, Qian CN and Zhang J: Wnt3a: Functions and implications in cancer. *Chin J Cancer* 34: 554-562, 2015.
39. Wang HS, Nie X, Wu RB, Yuan HW, Ma YH, Liu XL, Zhang JY, Deng XL, Na Q, Jin HY, *et al*: Downregulation of human Wnt3 in gastric cancer suppresses cell proliferation and induces apoptosis. *Oncotargets Ther* 27: 3849-3860, 2016.
40. Nakashima N, Liu D, Huang CL, Ueno M, Zhang X and Yokomise H: *Wnt3* gene expression promotes tumor progression in non-small cell lung cancer. *Lung Cancer* 76: 228-234, 2012.
41. Xing Z, Wang HY, Su WY, Liu YF, Wang XX, Zhan P, Lv TF and Song Y: Wnt3 knockdown sensitizes human non-small cell type lung cancer (NSCLC) cells to cisplatin via regulating the cell proliferation and apoptosis. *Eur Rev Med Pharmacol Sci* 22: 1323-1332, 2018.
42. Kim M, Lee HC, Tsedensodnom O, Hartley R, Lim YS, Yu E, Merle P and Wands JR: Functional interaction between Wnt3 and Frizzled-7 leads to activation of the Wnt/beta-catenin signaling pathway in hepatocellular carcinoma cells. *J Hepatol* 48: 780-791, 2008.
43. Nambotin SB, Tomimaru Y, Merle P, Wands JR and Kim M: Functional consequences of WNT3/Frizzled7-mediated signaling in non-transformed hepatic cells. *Oncogenesis* 22: e31, 2012.
44. Zhang J, Gill AJ, Issacs JD, Atmore B, Johns A, Delbridge LW, Lai R and McMullen TP: The Wnt/ $\beta$ -catenin pathway drives increased cyclin D1 levels in lymph node metastasis in papillary thyroid cancer. *Hum Pathol* 43: 1044-1050, 2012.
45. Bronte V and Zanovello P: Regulation of immune responses by L-arginine metabolism. *Nat Rev Immunol* 5: 641-654, 2005.
46. Rodriguez PC, Quiceno DG, Zabaleta J, Ortiz B, Zea AH, Piazuelo MB, Delgado A, Correa P, Brayer J, Sotomayor EM, *et al*: Arginase I production in the tumor microenvironment by mature myeloid cells inhibits T-cell receptor expression and antigen-specific T-cell responses. *Cancer Res* 64: 5839-5849, 2004.
47. Boutard V, Havouis R, Fouqueray B, Philippe C, Moulinoux JP and Baud L: Transforming growth factor- $\beta$  stimulates arginase activity in macrophages. Implications for the regulation of macrophage cytotoxicity. *J Immunol* 155: 2077-2084, 1995.
48. Morrison AC and Correll PH: Activation of the stem cell derived tyrosine kinase/RON receptor tyrosine kinase by macrophage-stimulating protein results in the induction of arginase activity in murine peritoneal macrophages. *J Immunol* 168: 853-860, 2002.
49. Jost MM, Ninci E, Meder B, Kempf C, Van Royen N, Hua J, Berger B, Hoefler I, Modolell M and Buschmann I: Divergent effects of GM-CSF and TGF $\beta$  on bone marrow-derived macrophage arginase-1 activity, MCP-1 expression, and matrix metalloproteinase-12: A potential role during arteriogenesis. *FASEB J* 17: 2281-2283, 2003.
50. Qiu F, Huang J and Sui M: Targeting arginine metabolism pathway to treat arginine-dependent cancers. *Cancer Lett* 364: 1-7, 2015.
51. Fultang L, Vardon A, De Santo C and Mussai F: Molecular basis and current strategies of therapeutic arginine depletion for cancer. *Int J Cancer* 139: 501-509, 2016.
52. Huang X, Ding L, Bennewith KL, Tong RT, Welford SM, Ang KK, Story M, Le QT and Giaccia AJ: Hypoxia inducible mir-210 regulates normoxic gene expression involved in tumor initiation. *Mol Cell* 35: 856-867, 2009.
53. Dang K and Myers KA: The role of hypoxia-induced miR-210 in cancer progression. *Int J Mol Sci* 16: 6353-6372, 2015.
54. Ying Q, Liang L, Guo W, Zha R, Tian Q, Huang S, Yao J, Ding J, Bao M, Ge C, *et al*: Hypoxia-inducible microRNA-210 augments the metastatic potential of tumor cells by targeting vacuole membrane protein 1 in hepatocellular carcinoma. *Hepatology* 54: 2064-2075, 2011.

